Acta Cryst. (1992). A48, 655-663

Bragg–Surface Three-Beam Dynamical X-ray Diffraction

BY CHUNG-YUAN JEN AND SHIH-LIN CHANG

Department of Physics, National Tsing Hua University, Hsinchu 30043, *Taiwan*

(*Received* 5 *November* 1991; *accepted* 25 *February* 1992)

Abstract

Three-beam diffraction with a symmetric Bragg reflection and a surface diffraction is studied based on the dynamical theory of X-ray diffraction. The difficulty involved in the boundary conditions for the surface diffraction is overcome by treating the Bragg-surface diffraction as either a Bragg-Laue or a Bragg-Bragg case with the inclination angle α between the crystal surface and the surface-diffracted beam being very small, about 10^{-5} rad. The geometry of the dispersion surface, the number of permitted modes of wave propagation, the linear absorption coefficient, the excitation of the beam and the diffracted intensity are calculated for the Ge (000) (222) (31$\bar{1}$) Bragg-surface diffraction of Cu $K\alpha_1$. It is found that the calculated relative integrated intensity ratio among the Bragg-surface 31$\bar{1}$ case and the Bragg-Bragg 113 and 51$\bar{1}$ cases is in good agreement with the integrated intensity ratio obtained experimentally.

1. Introduction

Multiple diffraction takes place when several sets of atomic planes are simultaneously in a position to diffract an incident X-ray beam. In terms of the reciprocal lattice, several reciprocal-lattice points are simultaneously on the surface of the Ewald sphere. In the case of a symmetric three-beam (O, G, L) diffraction (Fig. 1), there are three reciprocal-lattice points O, G and L involved, and the G reflection is a symmetric Bragg reflection (the primary reflection). O is the origin of the reciprocal lattice and also represents the direct incident beam. The vector $\overrightarrow{OG}(=\mathbf{g})$ and $\overrightarrow{OL}(=\mathbf{l})$ are the reciprocal-lattice vectors of the G and L reflections, respectively. θ_G is the Bragg angle of the G reflection. $\mathbf{K}_O$, $\mathbf{K}_G$ and $\mathbf{K}_L$ are the wave vectors of the O, G and L diffractions. For the symmetric G reflection the crystal surface is parallel to the G atomic planes. The equatorial plane of the Ewald sphere bisecting the vector $\mathbf{g}$ represents the crystal surface in real space. If the reciprocal-lattice point L of the (secondary) L reflection lies above or below the equatorial plane, then the L reflection is of a Bragg or Laue type. The three-beam case of the former is called the Bragg-Bragg, the latter the Bragg-Laue diffraction. If the L point is in the equatorial plane, as shown in Fig. 1, then the diffracted beam of the L reflection travels along the crystal surface. In this case, the three-beam case is called a Bragg-surface diffraction, because it involves a symmetric Bragg reflection G and a surface reflection L.

The intensities of both Bragg-Bragg and Bragg-Laue three-beam diffractions can be calculated based on the dynamical theory of X-ray diffraction without difficulties. As to the Bragg-surface case, it is, however, difficult to set up exact and useful boundary conditions for the surface-propagating waves. It is therefore the aim of this paper to solve this problem by using a small-angle approximation for the surface-diffracted waves, *i.e.* a small angle α is introduced between the surface-diffracted beam and the crystal surface. The surface-diffracted intensity is then calculated as the asymptotic value for the α angle approaching zero. In addition, the number of modes of wave propagation is considered for this special surface reflection. The coordinates of the tie points on the dispersion surface, the absorption coefficients

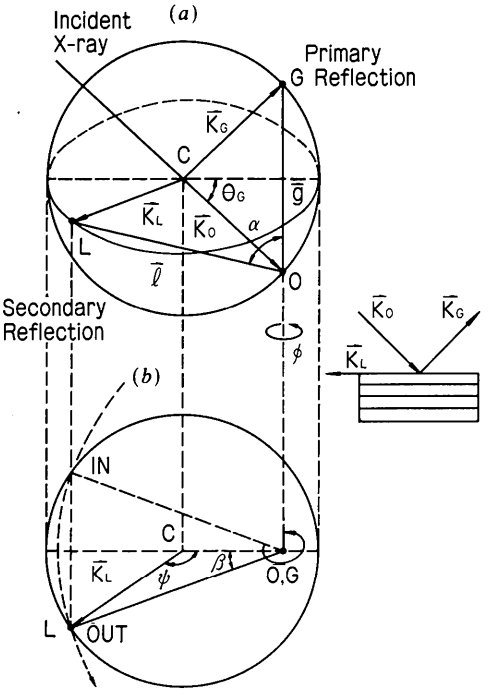

Fig. 1. Geometry of a Bragg-surface three-beam diffraction: (*a*) overview; (*b*) top view.

0108-7673/92/050655-09$06.00

and the excitation of modes are also given. Experimentally, the intensities of the three-beam Bragg-surface case of Ge (000) (222) (31$\bar{1}$) and the Bragg-Bragg cases, Ge (000) (222) (113) and Ge (000) (222) (51$\bar{1}$), for Cu $K\alpha_1$ radiation are measured and compared with the calculated ones. It should be noted that the coplanar type of multiple diffraction has been reported by Graeff & Bonse (1977) and Pacherova & Bubakova (1987), where the dispersion equation can be solved analytically. In the present paper, we are dealing with a noncoplanar Bragg-surface diffraction, where an analytical solution of the dispersion equation does not exist.

2. Theoretical considerations

For a three-beam (O, G, L) diffraction, the fundamental equation of wave fields for both σ and π polarizations takes the matrix form

$$[\tilde{\Phi}][\mathbf{D}]=0, \tag{1}$$

where

$$[\tilde{\Phi}]=\begin{bmatrix} \chi_O-2\varepsilon_O & 0 & P_\sigma\chi_{\bar{G}} & 0 & d_2\chi_{\bar{L}} & 0 \\ 0 & \chi_O-2\varepsilon_O & 0 & P_\pi\chi_{\bar{G}} & d_1\chi_{\bar{L}} & d_3\chi_{\bar{L}} \\ P_\sigma\chi_G & 0 & \chi_O-2\varepsilon_G & 0 & d_2\chi_{G-L} & 0 \\ 0 & P_\pi\chi_G & 0 & \chi_O-2\varepsilon_G & d_1'\chi_{G-L} & d_3\chi_{G-L} \\ d_2\chi_L & d_1\chi_L & d_2\chi_{L-G} & d_1'\chi_{L-G} & \chi_O-2\varepsilon_L & 0 \\ 0 & d_3\chi_L & 0 & d_3'\chi_{L-G} & 0 & \chi_O-2\varepsilon_L \end{bmatrix} \tag{2}$$

and the column vector $[\mathbf{D}]$ is expressed horizontally as

$$[\mathbf{D}]=[D_{\sigma O}\, D_{\pi O}\, D_{\sigma G}\, D_{\pi G}\, D_{\sigma L}\, D_{\pi L}]. \tag{3}$$

$\chi_G/4\pi$ is the electric susceptibility of the G reflection. $\chi_G=\Gamma F_G=-(r_e\lambda^2/\pi v)F_G$, F_G being the structure factor, r_e the classical radius of the electron and v the volume of the crystal unit cell. The quantity 2ε is defined as

$$2\varepsilon_H=(K_H^2-k^2)/k^2 \tag{4}$$

for $H=O$, G and L. $\mathbf{K}_H$ is the wave vector of the H reflection inside the crystal and k is the magnitude of the wave vector in vacuum: $\mathbf{K}_O=\overrightarrow{CO}$, $\mathbf{K}_G=\overrightarrow{CG}$ and $\mathbf{K}_L=\overrightarrow{CL}$ (see Figs. 1 and 2). They are related to the wave vectors $\mathbf{k}_O$, $\mathbf{k}_G$ and $\mathbf{k}_L$ in vacuum by

$$\mathbf{K}_H=\mathbf{k}_H-k\delta\hat{\mathbf{n}} \tag{5}$$

where $k\delta$ is the accommodation and $\hat{\mathbf{n}}$ the unit vector of the surface inward normal. In terms of the dynamical theory, point C in Fig. 2 is the tie point on the dispersion surface, which defines the wave vectors $\mathbf{K}_H$. $\mathbf{k}_H$, depending on the entrance point, are functions of $\Delta\theta$ and φ, $\Delta\theta$ being the angular deviation from the Bragg angle θ_G and φ the exact three-beam position of the azimuth angle around $\mathbf{g}$. For simplicity, we adopt the geometrical expressions for $\mathbf{k}_H$ and $\mathbf{K}_H$ from Chang (1984). Since the derivation of these expressions is purely geometrical and straightforward, we will not present here the explicit forms of $\mathbf{K}_H$. For later discussion, we choose the origin (zero point) of the coordinates of tie points on the dispersion surface at the Laue point, *i.e.* $k_O=k_G=k_L=1/\lambda$, $\Delta\theta=0$, $\varphi=0$ and the y axis is along the $\hat{\mathbf{n}}$ direction.

The σ- and π-polarized components of the wave fields, $\mathbf{D}_\sigma$ and $\mathbf{D}_\pi$, are defined according to the $\hat{\boldsymbol{\sigma}}$ and $\hat{\boldsymbol{\pi}}$ unit vectors shown in Fig. 2. Accordingly, the polarization factors P and d can be expressed in terms of the scalar products of these polarization unit vectors,

$$P_\sigma=\hat{\boldsymbol{\sigma}}_O\cdot\hat{\boldsymbol{\sigma}}_O=1 \qquad P_\pi=\hat{\boldsymbol{\pi}}_O\cdot\hat{\boldsymbol{\pi}}_G=\cos 2\theta_G$$

$$d_1=\hat{\boldsymbol{\pi}}_O\cdot\hat{\boldsymbol{\sigma}}_L=-\sin\psi\sin\theta_G$$

$$d_2=\hat{\boldsymbol{\sigma}}_O\cdot\hat{\boldsymbol{\sigma}}_L=\hat{\boldsymbol{\sigma}}_G\cdot\hat{\boldsymbol{\sigma}}_L=\cos\psi$$

$$d_3=\hat{\boldsymbol{\pi}}_O\cdot\hat{\boldsymbol{\pi}}_L=\cos\theta_G \qquad d_1'=\hat{\boldsymbol{\pi}}_G\cdot\hat{\boldsymbol{\sigma}}_L=\sin\psi\sin\theta_G$$

$$d_3'=\hat{\boldsymbol{\pi}}_G\cdot\hat{\boldsymbol{\pi}}_L=\cos\theta_G$$

$$\hat{\boldsymbol{\sigma}}_O\cdot\hat{\boldsymbol{\pi}}_O=\hat{\boldsymbol{\sigma}}_O\cdot\hat{\boldsymbol{\pi}}_L=\hat{\boldsymbol{\pi}}_O\cdot\hat{\boldsymbol{\sigma}}_G=\hat{\boldsymbol{\sigma}}_G\cdot\hat{\boldsymbol{\pi}}_L=\hat{\boldsymbol{\sigma}}_O\cdot\hat{\boldsymbol{\pi}}_G=0,$$

where ψ is the angle between OL and the COG plane.

(*a*) *Number of permitted modes of wave propagation*

Equation (1) can be solved as an eigenvalue equation. For a general N-beam diffraction there are $2N$ eigenvalues corresponding to $2N$ modes of wave propagation. If the crystal is thick, for example $\mu t>10$, where μ is the linear absorption coefficient and t is the crystal thickness, and no grazing incidence or surface reflection is involved, the number N_P of permitted modes is

$$N_P=2(N-N_B) \tag{6}$$

where N_B is the number of Bragg reflected beams (Pinsker, 1977; Chang, 1979).

Equation (6) is certainly not valid for cases involving surface reflections. However, the surface case can be treated as an extreme case of either Bragg-Laue

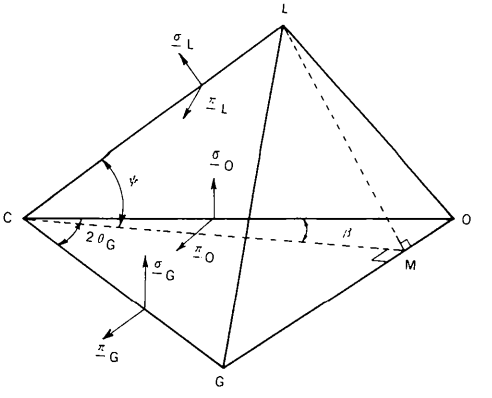

Fig. 2. Definition of the polarization unit vectors. All $\hat{\boldsymbol{\pi}}$ are parallel to the OCG plane and the $\hat{\boldsymbol{\sigma}}$ satisfy $\hat{\boldsymbol{\sigma}}_M\times\hat{\boldsymbol{\pi}}_M=\hat{\mathbf{K}}_M$ ($\mathbf{K}_M=\overrightarrow{CM}$) for $M=O$, G and L.

or Bragg–Bragg diffraction with the angle α, between the surface diffracted beam and the crystal surface, approaching zero. Figs. 3(a) and (b) show schematically the diffraction geometry of Bragg–Bragg ($\alpha > 0$) and Bragg–Laue ($\alpha < 0$) cases. It should be noted that in Fig. 3(b) the surface-transmitted beam, represented by the wave vector $\mathbf{K}_L$, is accompanied by a grazing (specular) reflected beam $\mathbf{k}_L^s$. In the following, we shall follow the procedure of Chang (1979) to determine the number of permitted modes involved in these particular three-beam diffractions.

Equation (5) for a given mode j of wave propagation may be rewritten as

$$\mathbf{K}_{Gj} = \mathbf{k}_{Gj} - k\delta_j \hat{\mathbf{n}}, \tag{7}$$

where $\mathbf{K}$, $\mathbf{k}$ and δ_j are complex and $k = 1/\lambda$. Accordingly, $2\varepsilon_{Gj}$ can be written as

$$2\varepsilon_{Gj} = [(\mathbf{k}_{Gj} - k\delta_j \hat{\mathbf{n}})^2 - k^2]/k, \tag{8}$$

which leads to

$$2\varepsilon_{Gj} = -2\gamma_{Gj}\delta_j + O(\delta_j^2) \tag{9}$$

for ordinary G reflection, where the second-order term $|O(\delta_j^2)| \ll |2\gamma_G \delta_j|$ and

$$2\varepsilon_{Lj} = -2\alpha\delta_j + \delta_j^2 \tag{10}$$

for a grazing surface reflection L, where $|2\alpha\delta_j| \simeq |\delta_j^2|$. γ_G is the direction cosine of the $\mathbf{k}_G$ with respect to $\hat{\mathbf{n}}$, *i.e.* $\gamma_G = \hat{\mathbf{k}}_G \cdot \hat{\mathbf{n}}$.

To satisfy the requirement of conservation of total energy, the imaginary part δ^i of δ must be non-negative for a permitted mode. According to Chang (1979), the number of permitted modes of propagation is the number of positive δ^i, which can be determined based on Descartes's rule of signs. Since the electric susceptibility of the incident reflection is always greater than the diffracted ones, *i.e.* $|\chi_O^r| > |\chi_H^r|$ for $H = G$ and L (the superscript r indicates the real part) and the sign of δ^i is the same as the sign of δ^r at the exact N-beam diffraction position, the signs of δ^r are independent of the off-diagonal elements of the square matrix $[\tilde{\Phi}]$ of (2). Therefore, the determinant of $[\tilde{\Phi}]$ takes the form

$$[\tilde{\Phi}] = \prod_{j=1}^{N_O} (\chi_O + 2\gamma_G\delta)^2(\chi_O + 2\alpha\delta - \delta^2)^2 = 0 \tag{11}$$

for an N-beam diffraction in which there are N_O ordinary reflections and one surface-reflected reflection. Obviously, the solutions of the quadratic equation related to surface diffraction are

$$\delta = -\alpha \pm (\chi_O^2 + \alpha)^{1/2} \tag{12}$$

where only one root satisfies the conservation of energy, no matter what the sign of α. This fact indicates that the three-beam Bragg–surface case studied can be treated as either a Bragg–Bragg or a Bragg–Laue case and the number of permitted modes in both cases is four [*i.e.* $2(N - N_B) + 2 = 4$].

(b) *Boundary conditions of wave-field amplitudes*

By considering the number of permitted modes and the eigenvalue equation (1), the coordinates of the tie point on the dispersion surface can be determined from the real part δ^r of the eigenvalue, while the linear absorption coefficient is related to the imaginary part δ^i. The eigenvectors provide the ratios of the wave-field amplitudes involved. The absolute wave-field amplitudes can be determined by the boundary conditions, *i.e.* the continuities of the normal components of the electric displacements and the tangential components of the magnetic fields at the crystal boundary, respectively (Afanas'ev & Melkonyan, 1983), are

$$\begin{aligned} \sum_{j=1}^{4} D_{\sigma O}(j) &= E_{\sigma O} & \sum_{j=1}^{4} D_{\pi O}(j) &= E_{\pi O} \\ \sum_{j=1}^{4} D_{\sigma G}(j) &= E_{\sigma G} & \sum_{j=1}^{4} D_{\pi G}(j) &= E_{\pi G} \\ \sum_{j=1}^{4} D_{\sigma L}(j) &= E^s_{\sigma L} & \sum_{j=1}^{4} D_{\pi L}(j) &= E^S_{\pi L} \end{aligned} \tag{13}$$

and

$$\begin{aligned} \sum_{j=1}^{4} u_L(j) D_{\sigma L}(j) &= -|\alpha| E^S_{\sigma L} \\ \sum_{j=1}^{4} u_L(j) D_{\pi L}(j) &= -|\alpha| E^S_{\pi L} \end{aligned} \tag{14}$$

for the Bragg–Laue ($\alpha < 0$) geometry. $E_{\sigma H}$ and $E_{\pi H}$ are the σ and π components of the electric field of the H-reflected wave in vacuum ($H = O$, G or L), while $E^S_{\sigma L}$ and $E^S_{\pi L}$ are those of the surface-reflected wave. The parameter u is defined as $u_L = K_{Lz}/k$, K_{Lz} being the component of $\mathbf{K}_L$ normal to the crystal

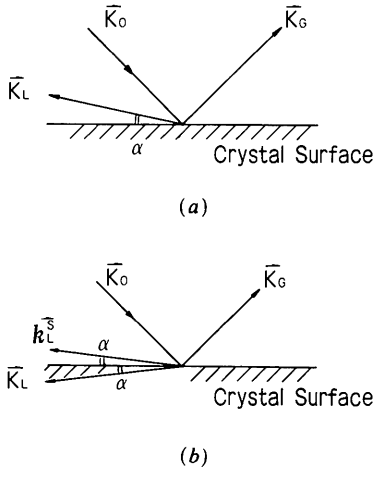

Fig. 3. Schematic representation of (a) Bragg–Bragg ($\alpha > 0$) and (b) Bragg–Laue ($\alpha < 0$) diffractions.

surface. For the Bragg-Bragg geometry ($\alpha > 0$), the boundary conditions remain the same as (13) and (14), except that $E^S_{\sigma L}$ and $E^S_{\pi L}$ are replaced by $E_{\sigma L}$ and $E_{\pi L}$.

Since the σ- and π-polarized wave fields are correlated with each other in three-beam diffraction, *i.e.* $\hat{\boldsymbol{\sigma}}_O$ is not necessarily perpendicular to $\hat{\boldsymbol{\pi}}_L$, the excitations of $E_{\sigma L}$ by both $E_{\sigma O}$ and $E_{\pi O}$ may not be null (Chang, 1984); $E_{\sigma L}(\sigma) \neq 0$ and $E_{\sigma L}(\pi) \neq 0$. To include this correlated excitation, each equation in the boundary conditions should be decomposed into two parts to relate to the contributions from the excitations by $E_{\sigma O}$ and $E_{\pi O}$. The boundary conditions of (13) and (14) can then be written as

$$\begin{aligned}
&\sum_{j=1}^{4} C_{\sigma O}(j)X_\sigma(j) = E_{\sigma O} \qquad \sum_{j=1}^{4} C_{\sigma O}(j)X_\pi(j) = 0\\
&\sum_{j=1}^{4} C_{\sigma G}(j)X_\sigma(j) = E_{\sigma G}(\sigma)\\
&\sum_{j=1}^{4} C_{\sigma G}(j)X_\pi(j) = E_{\sigma G}(\pi)\\
&\sum_{j=1}^{4} C_{\sigma L}(j)X_\sigma(j) = E^S_{\sigma L}(\sigma)\\
&\sum_{j=1}^{4} C_{\sigma L}(j)X_\pi(j) = E^S_{\sigma L}(\pi)\\
&\sum_{j=1}^{4} u_L(j)C_{\sigma L}(j)X_\sigma(j) = -|\alpha|E^S_{\sigma L}(\sigma)\\
&\sum_{j=1}^{4} u_L(j)C_{\sigma L}(j)X_\pi(j) = -|\alpha|E^S_{\sigma L}(\pi) \qquad (15)
\end{aligned}$$

for the σ components. Similarly, there are eight equations of the same form as (15) for the π components. The quantities $C_{\sigma H}(j)$ and $C_{\pi H}(j)$ are the amplitude ratios defined as

$$\begin{aligned}
C_{\sigma H}(j) &= D_{\sigma H}(j)/X_\sigma(j)\\
C_{\pi H}(j) &= D_{\pi H}(j)/X_\pi(j),
\end{aligned} \qquad (16)$$

where $X_{\sigma,\pi}$ are the proportional constants, which can be found from (15). Hence the D_H are determined *via* (16). The intensity of the G reflection is therefore given by

$$I_G = [|E_{\sigma G}(\sigma) + E_{\sigma G}(\pi)|^2 + |E_{\pi G}(\sigma)E_{\pi G}(\pi)|^2]/|E_O|^2, \qquad (17)$$

where

$$|E_O|^2 = |E_{\sigma O}|^2 + |E_{\pi O}|^2. \qquad (18)$$

The excitation of mode, $\mathrm{Ex}(j)$, and the excitation of beam, $\mathrm{Ex}(H)$, can be calculated as

$$\mathrm{Ex}(j) = \sum_{H=O,G,L} [|D_{\sigma H}(j)|^2 + |D_{\pi H}(j)|^2]/|E_O|^2 \qquad (19)$$

$$\mathrm{Ex}(H) = \sum_{j=1}^{4} [|D_{\sigma H}(j)|^2 + |D_{\pi H}(j)|^2] \times (\sin\theta_H)/(|E_O|^2 \sin\theta_G), \qquad (20)$$

where $\sin\theta_H/\sin\theta_G$ is the ratio of the direction cosines of the H and O defracted beams. Clearly, $\mathrm{Ex}(H)$ is simply the H component of the Poynting vector. The linear absorption coefficient of mode j is defined as

$$\mu(j) = 4\pi k\delta^i_j. \qquad (21)$$

All the terms mentioned in (13)-(21) are the expressions for a given $\Delta\theta$ and φ.

3. Numerical calculations

Dynamical calculations following the above theoretical considerations are carried out for the three-beam Bragg-surface diffraction, *i.e.* Ge (000) (222) ($31\bar{1}$) for Cu $K\alpha_1$, where 222 is a symmetric Bragg reflection and $31\bar{1}$ is a surface diffraction. To solve the nonlinear equation of (2), the *REDUCE* program (Hearn, 1987) was used to calculate the complex roots δ^r. The atomic scattering factors, temperature factors and anomalous scattering corrections used were obtained from *International Tables for X-ray Crystallography* (1974).

(*a*) *Dispersion surface*

Fig. 4 shows the dispersion sheets at $\Delta\theta = 0$ for different inclination angles $\pm\alpha$. The abscissa is the azimuthal angle φ deviated from the exact three-beam position $\varphi = 0$ and the ordinate represents the y coordinate of the tie point C along the $-\hat{\mathbf{n}}$ direction. The Laue point is at $y = 0$ and $\varphi = 0$, $\Delta\theta = 0$. There are four curves corresponding to the four modes of propagation. The dispersion curves of modes 1 and 2 are almost identical. They are related to the terms involving the surface inclination angle α in (12). Those of modes 3 and 4 are attributed to the first term on the right-hand side of (11), which depends on the direction cosine γ_O of the direct beam. The drastic change of the dispersion curves of modes 3 and 4 occurs when the three-beam interaction comes into play at $\varphi = 24''$. As can be seen in Fig. 4, the separation between modes 1 and 3 is related to the α angle. The dispersion curves of mode 1 are lower for $\alpha = -10^3$ μrad and higher for $\alpha = 10^3$ μrad than those of mode 3. The relative positions of the dispersion curves of modes 1, 2, 3 and 4 remain unchanged as α approaches zero. Thus, Figs. 4(*e*) and (*f*) show that the dispersion surfaces for $\alpha = \pm 10$ μrad are practically identical. Based on this fact, we could safely treat the dispersion surface at $|\alpha| = 10$ μrad as that for the three-beam Bragg-surface diffraction.

The dispersion surfaces with $|\alpha| = 10$ μrad at $\Delta\theta =$ 0, 38.3 and 76.6 μrad are calculated to demonstrate the effect of the total reflection on the position of the dispersion curves. The cuts at $\Delta\theta = 0$ and 76.6 μrad are the two sections before and after the total reflection, while the section at $\Delta\theta = 38.3$ μrad goes through the Lorentz point, the center of the total reflection

range. Fig. 5 clearly shows that the three-beam interaction points appearing in curves 3 and 4 are shifted from 24 μrad for $\Delta\theta = 0$ to 52 μrad for $\Delta\theta = 38.3$ μrad and to 80 μrad for $\Delta\theta = 76.6$ μrad. It is interesting to note that the dispersion curve of mode 4 at the Lorentz point is a straight line. This implies that mode 4 is not sensitive to the three-beam interaction so that it maintains its two-beam character at the Lorentz point.

(*b*) *Absorption and excitation*

Fig. 6 presents the linear absorption coefficients μ for $\alpha = \pm 10$ μrad. Again, this demonstrates that, with $|\alpha| = 10$ μrad, both the Bragg–Laue and Bragg–Bragg cases behave as if they were Bragg-surface diffractions. As clearly shown in Fig. 6, the abnormally large absorption of modes 1 and 2 is due to the large imaginary part of $(\chi_O^2 + \alpha)^{1/2}$ in (12),

$$\delta \simeq \alpha \pm (-\tfrac{1}{2}|\chi_O^i/|\chi_O^r|^{1/2}| + i|\chi_O^r|^{1/2}). \qquad (22)$$

It is understandable that the modes physically associated with a shallow diffracted beam suffer more absorption than those with the ordinary diffracted beam. However, these two modes (1 and 2) are actually not excited at all in the diffraction process as can be seen in the excitations of the 000, 222 and $31\bar{1}$ beams shown in Figs. 7, 8 and 9, respectively. The excitations of modes 3 and 4 are similar. Strong excitation takes place at the three-beam point. The excitation of mode 4 is stronger than that of mode 3 since the dispersion curve of mode 4 is relatively closer to the Laue point than that of mode 3. Therefore, mode 4, according to Ewald & Heno (1968), is excited more than mode 3 by the incident wave. Consequently, the absorption of the former is less than that of the latter (Fig. 6). The excitation of the $31\bar{1}$ beam, which has two peaks (or two kinks), is quite different from the excitation of the 222 beam. These two peaks occur when crossing the total reflection range of the $31\bar{1}$ reflection. The positions of the peaks correspond to the projected positions of the

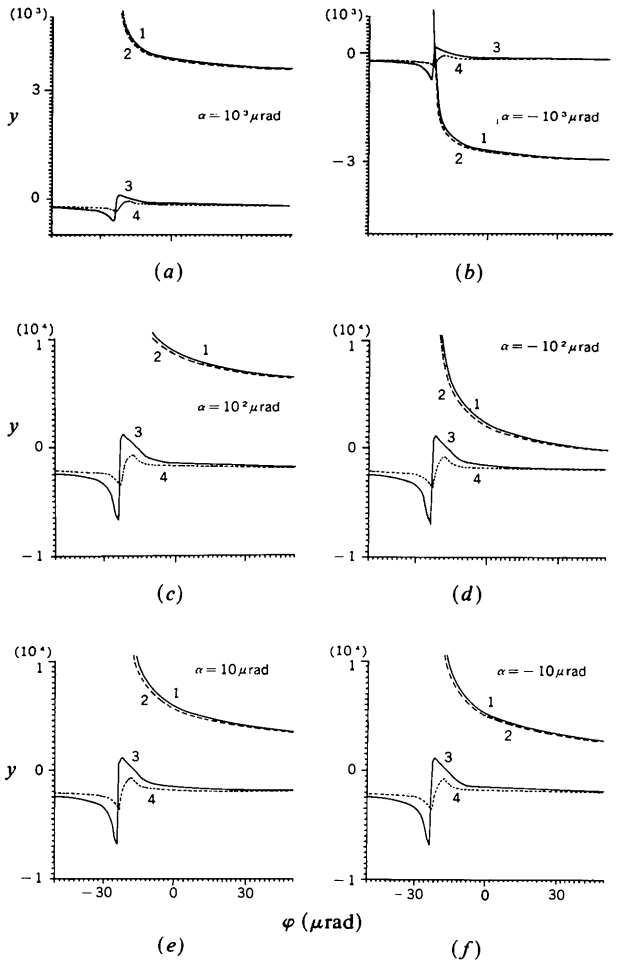

Fig. 4. Dispersion curves, Y (cm^{-1}) *versus* φ (μrad), of modes 1-4 at $\Delta\theta = 0$ with various α values for Ge (000) (222) ($31\bar{1}$) Cu $K\alpha_1$.

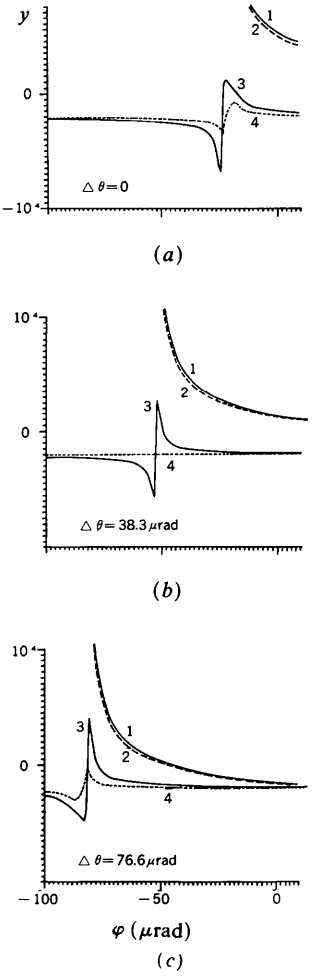

Fig. 5. Dispersion curves, Y (cm^{-1}) *versus* φ (μrad), of modes 1-4 at (*a*) $\Delta\theta = 0$; (*b*) $\Delta\theta = 38.3$ μrad and (*c*) $\Delta\theta = 76.6$ μrad ($\alpha = 10$ μrad).

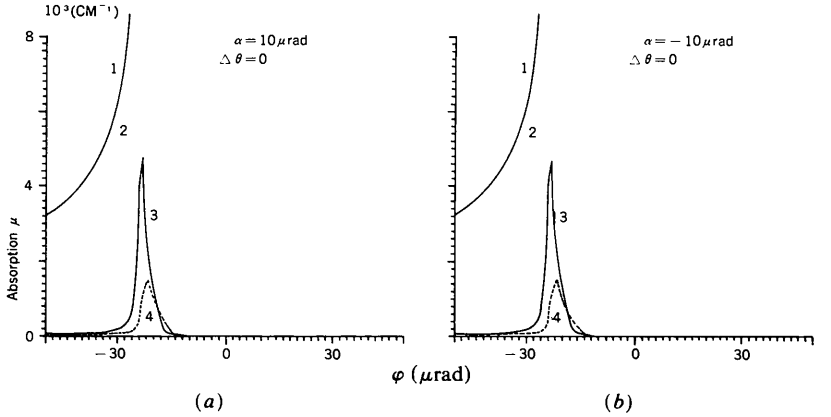

Fig. 6. Linear absorption coefficients of modes 1-4 at $\Delta\theta = 0$: (*a*) $\alpha = 10$ μrad; (*b*) $\alpha = -10$ μrad.

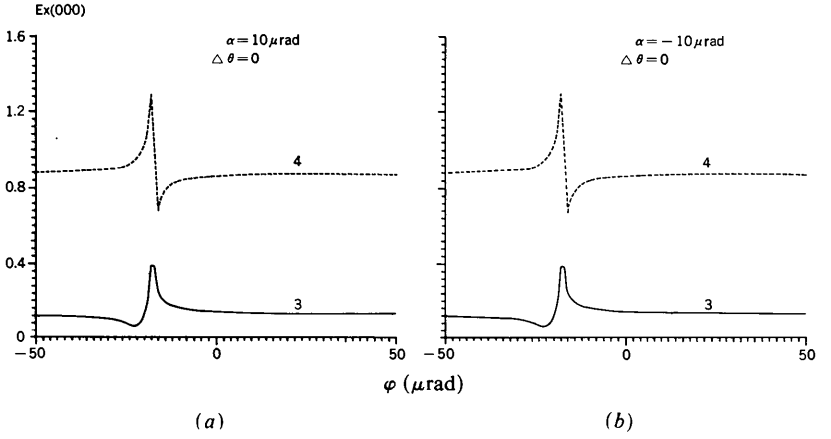

Fig. 7. Excitations of the 000 beam for modes 1-4 at $\Delta\theta = 0$ and $\alpha = \pm 10$ μrad.

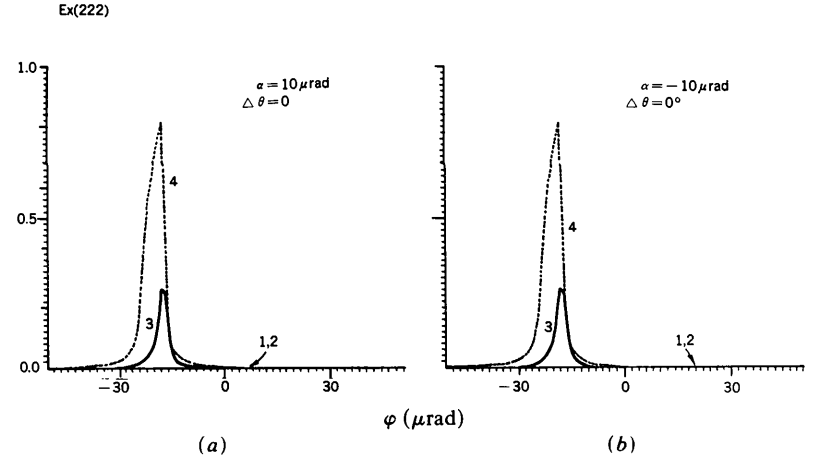

Fig. 8. Excitations of the 222 beam for modes 1-4 at $\Delta\theta = 0$ and $\alpha = \pm 10$ μrad.

two branches of the dispersion hyperbola onto the φ axis. For the 222 reflection, the cut at $\Delta\theta = 0$ is only on one branch of the 222 dispersion hyperbola. Therefore, Ex(222) has only a single peak for each mode. Moreover, it is not surprising to see that Ex(31$\bar{1}$) is much less than Ex(222) because the surface diffraction is usually weakly excited.

(*c*) *Intensity*

The intensity at given $\Delta\theta$ and φ is calculated according to (18) for the relative 222 intensity, denoted as $I(31\bar{1})/I(000)$. The integrated intensity over $\Delta\theta$ and φ is also calculated for each φ position. The integration range is 0.03° for $\Delta\theta$ and φ, which corresponds to the beam divergence used in the experiment (see § 4). Fig. 10 shows the calculated integrated intensity *versus* φ for the Bragg-surface case 31$\bar{1}$ (with $\alpha = 10$ μrad) and two Bragg-Bragg cases, 113 and 51$\bar{1}$. The latter are calculated according to the wide-angle geometry (see, for example, Chang, 1984). The purpose of calculating these three cases is to obtain a relative intensity ratio that can be compared with the experimentally measured intensities. The total integrated intensities, I over φ, of the 31$\bar{1}$ case are also calculated for various α. They are plotted on an arbitrary scale in Fig. 11. Fig. 11 also indicates that the integrated 31$\bar{1}$ intensity approaches the asymptotic value as α nears 0°. In other words, the intensity calculated for $|\alpha| = 10$ μrad is very close to the surface (asymptotic) values.

4. Experimental

Multiple-diffraction experiments were performed on a Huber four-circle diffractometer (model 400) with Cu $K\alpha_1$ radiation from a rotating-anode X-ray generator. The set-up has previously been reported (Tang & Chang, 1988). The beam divergences are 0.03° in $\Delta\theta$ and φ. A germanium crystal was first aligned for the 222 reflection and then rotated around the [222] direction to bring in 31$\bar{1}$, 113 and 51$\bar{1}$ reflections at different φ positions. The detector always monitored

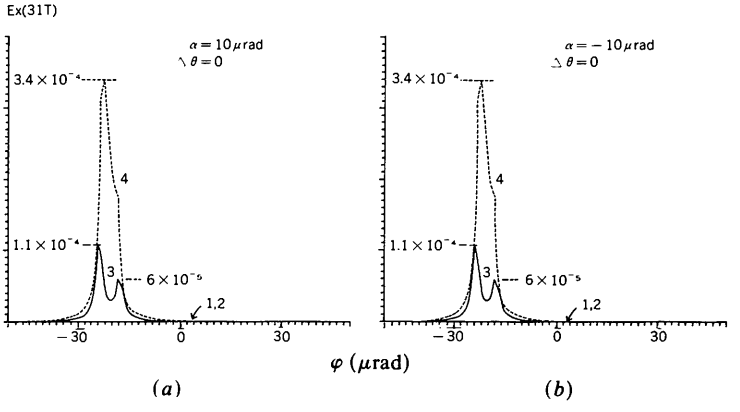

Fig. 9. Excitations of the 31$\bar{1}$ beam for modes 1-4 at $\Delta\theta = 0$ and $\alpha = \pm 10$ μrad.

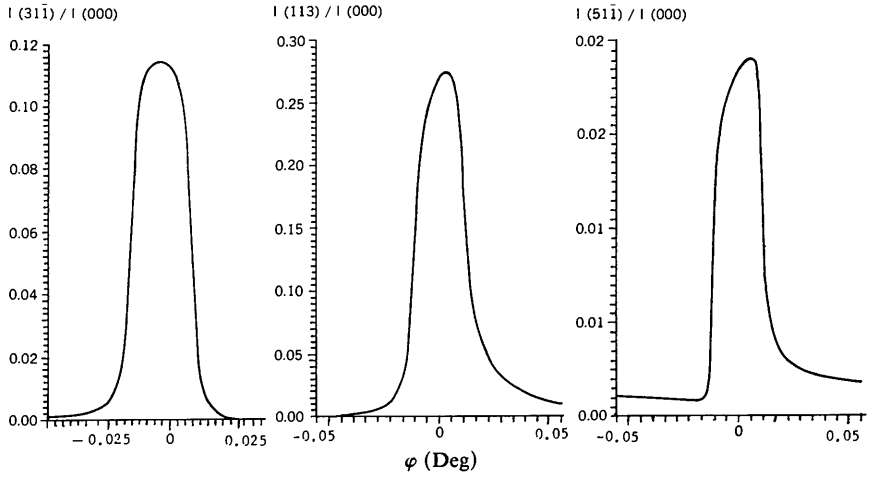

Fig. 10. Calculated integrated intensities *versus* φ for the Bragg-surface 31$\bar{1}$ and Bragg-Bragg 113 and 51$\bar{1}$ cases for Cu $K\alpha_1$.

the 222 reflected intensity. The φ scans with 0.01° per step in the vicinity of the Bragg-surface $31\bar{1}$ and the Bragg-Bragg 113 and $51\bar{1}$ cases were performed and the 222 reflected intensities in these positions are shown in Fig. 12.

5. Results and concluding remarks

The total intensity ratio $I(31\bar{1}):I(113):I(51\bar{1})$ measured from Fig. 12 is 1 : 1.8 : 0.17, which is in good agreement with the calculated ratio, 1 : 2.4 : 0.17. There are several possible sources of error. (i) The crystal may not be ideally perfect so that the calculated intensity of the strong reflection 113 is larger than the measured value. (ii) The crystal surface may not be exactly parallel to the (222) planes. A slight miscut on the surface could affect the measured intensity of the Bragg-surface diffraction. (iii) There are two three-beam cases, $3\bar{3}5$ and $5\bar{3}1$ (see Fig. 12), near the $31\bar{1}$ diffraction. Their presence should in principle modify the $31\bar{1}$ reflected intensity to some extent.

Aside from the slight disagreement between the calculated and measured intensities, the calculated procedures presented in this paper can still be used to provide sufficient information about the intensity, dispersion surface, absorption and mode excitation.

In conclusion, we have demonstrated that the small-angle approximation with the proper boundary conditions could be used to deal with dynamical Bragg-surface multiple diffractions. Furthermore, the number of permitted modes of a three-beam Bragg-surface diffraction is four. This can be easily generalized, by following the argument given in (11), to

$$N_P = 2(N - N_B + N_S) \qquad (23)$$

where N_S is the number of surface reflections.

The authors are indebted to the National Science Council for the financial support through grant NSC 81-0208-M007-94Y. One of us, CYJ, gratefully

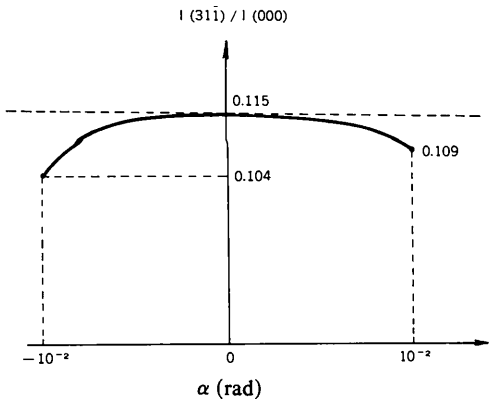

Fig. 11. Calculated total integrated intensity of the Bragg-surface $31\bar{1}$ diffraction *versus* α.

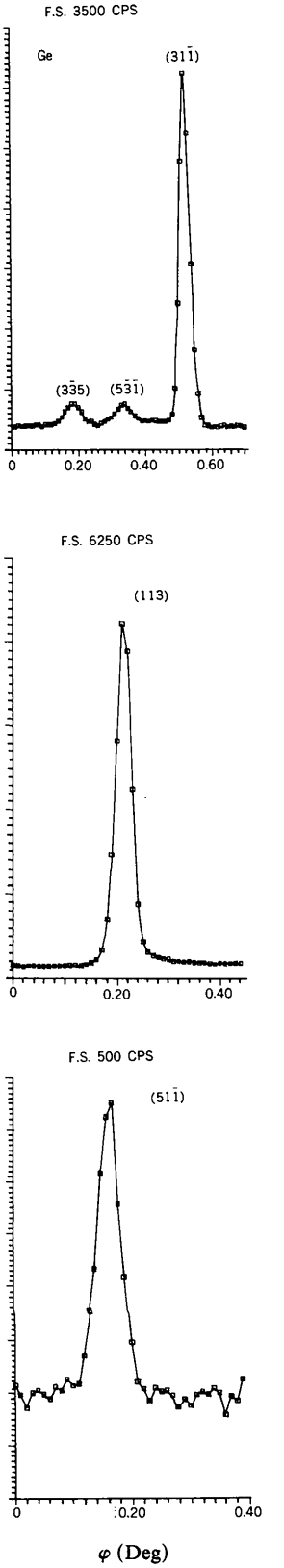

Fig. 12. Experimental intensity profiles for the Bragg-surface $31\bar{1}$ and Bragg-Bragg 113 and $51\bar{1}$ diffractions.

acknowledges the graduate fellowship provided by the same organization during the course of this study.

References

AFANAS'EV, A. M. & MELKONYAN, M. K. (1983). *Acta Cryst.* A**39**, 207-210.
CHANG, S. L. (1979). *Acta Cryst.* A**35**, 543-547.
CHANG, S. L. (1984). *Multiple Diffraction of X-rays in Crystals.* Berlin: Springer.
EWALD, P. P. & HENO, Y. (1968). *Acta Cryst.* A**24**, 5-15.
GRAEFF, W. & BONSE, U. (1977). *Z. Phys.* B**27**, 19-32.
HEARN, A. C. (1987). *The Algebraic Programming System REDUCE*, Version 3.3. The RAND corporation, Santa Monica, California, USA.
International Tables for X-ray Crystallography (1974). Vol. IV. Birmingham: Kynoch Press. (Present distributor Kluwer Academic Publishers, Dordrecht.)
PACHEROVA, O. & BUBAKOVA, R. (1987). *Acta Cryst.* A**43**, 161-167.
PINSKER, Z. G. (1977). *Dynamical Scattering of X-rays in Crystals.* Berlin, Heidelberg, New York: Springer.
TANG, M. T. & CHANG, S. L. (1988). *Acta Cryst.* A**44**, 1073-1078.

Acta Cryst. (1992). A**48**, 663-669

Uninodal 4-Connected 3D Nets. I. Nets without 3- or 4-Rings

BY M. O'KEEFFE AND N. E. BRESE

Department of Chemistry, Arizona State University, Tempe, AZ 85287, *USA*

(*Received* 29 *April* 1991; *accepted* 27 *January* 1992)

Abstract

A description is given of 4-connected nets with one kind of vertex in which the shortest rings containing each pair of edges are N-rings ($N>4$). Eleven uniform nets (6^6) are identified; seven of these are believed to be new. A further thirteen nets with one type of vertex and without 3- or 4-rings are described; nine of these are also believed to be new

Introduction

4-connected nets play an important role in crystal chemistry, notably as structures of elements and covalently bonded crystals and as the basis of the structures of hydrates, framework silicates and related materials. Considerable effort has been spent on enumerating possible structures and on characterizing their topologies; recent contributions that provide references to earlier work are those of Bosmans & Andries (1990) and Hansen (1990). In this series, some nets with all nodes congruent (uninodal) are described and analyzed topologically as a prelude to the development of a more complete topological theory of 4-connected nets than presently exists. With some reasonable geometrical restrictions (discussed below), the number of possible uninodal 4-connected nets is finite and we believe we have identified many of them. One motivation for this work is the belief that if we can discover how nature puts together simple nets, we can design more complicated nets by replacing single vertices by clusters of vertices (see, for example, Hansen, 1990).

Wells (1977) attached special significance to the uniform nets in which the shortest rings at every angle are equal in length. For uniform 4-connected nets, the rings at the six angles common to a vertex are all 6-rings (have six edges) and are symbolized 6^6. Wells in fact identified only three of these, of which two are the familiar diamond and lonsdaleite nets, and the third the structure of γ-silicon. Eleven are described here; we believe that seven of them have not been described before.

Most 4-connected nets found in crystal chemistry contain 3- or 4-rings. However, in addition to the uniform nets mentioned above, the familar nets of the quartz and NbO structures are examples of nets that contain only larger rings. Here we describe some other examples.

Terminology

A 4-connected net contains six angles defined by pairs of edges. Each angle has four others adjacent that share a common edge and one opposite that does not have a common edge. Each angle is contained in an N-circuit, which is a closed path (without retracing steps) of N edges from and returning to the reference vertex. A circuit is called a ring if, in addition, for every pair of vertices on the circuit, the path on the circuit between the vertices is a shortest path (*i.e.* there is no shortcut between them outside the circuit). Rings have been variously called 'fundamental circuits', 'primitive rings' and 'fundamental rings' by other authors. Goetzke & Klien (1991) have recently discussed nomenclature and different definitions used by different authors; their terminology is used here. For every net there is a finite number of rings for each vertex and their enumeration is of considerable

0108-7673/92/050663-07$06.00